Available online at www.sciencedirect.com
ScienceDirect
Trans. Nonferrous Met. Soc. China 33(2023) 2712−2725
Transactions of Nonferrous Metals Society of China
www.tnmsc.cn

Strengthening and thermal conductivity behaviors of cast Cu−La−Zn alloys

Bo HU[1], Jia-xuan HAN[1], De-jiang LI[1,2], Ming-di YU[1],
Jing-ya WANG[1], Xue-yang WANG[1], Zi-xin LI[1], Yu HUANG[3], Xiao-qin ZENG[1,2]

1. National Engineering Research Center of Light Alloy Net Forming, School of Materials Science and Engineering, Shanghai Jiao Tong University, Shanghai 200240, China;
2. State Key Laboratory of Metal Matrix Composites, Shanghai Jiao Tong University, Shanghai 200240, China;
3. Huawei Technologies Co., Ltd., Shenzhen 518129, China

Received 11 March 2022; accepted 29 April 2022

Abstract: A new Cu−La−Zn alloy system with high thermal conductivity was developed for die casting, and the thermal conductivity of this alloy system was 200−300 W/(m·K), which was twice as that of ordinary brass. The effects of Cu_6La intermetallic compounds and Zn solute atoms on the strengthening and thermal conductivity behaviors were quantitatively studied in as-cast binary Cu−La (2.0−4.5 wt.% La) and ternary Cu−2La−*x*Zn (0−3.0 wt.% Zn) alloys, respectively. The results showed that for the increase of per 1 wt.% La or Zn, the thermal conductivity decreased by about 34 W/(m·K). In Cu−2La−*x*Zn alloys, the lattice constant of α-Cu matrix increased from 3.6163 to 3.6239 Å. Due to the solid solution strengthening of Zn atoms, the hardness of the α-Cu matrix showed a parabolically increasing tendency, from 1.495 to 1.597 GPa. According to the calculations of the Maxwell−Eucken model based on the microstructure, the thermal conductivity of Cu_6La phase was determined to be about 35.37 W/(m·K), and the reduction in thermal conductivity of α-Cu matrix caused by Zn solute atoms was quantified to be 51.38 W/(m·K) per 1.0 at.% Zn increase.

Key words: Cu−La−Zn alloy; strengthening; thermal conductivity; intermetallic compound; solute atom

1 Introduction

With the high integration in 3C (computer, communication and consumer electronics), removing the excessive heat produced by the operation of electronic components and heat exchangers becomes more urgent, as overheating or deformation causes components to fail [1,2]. The demand for materials with both excellent heat dissipation and mechanical properties is increasing rapidly. High thermal conductivity copper alloys are considered to be the most promising candidate to solve this problem [3−5]. Casting, especially high-pressure die casting (HPDC), is a good choice for producing complex thin-walled electronic component structural parts [6]. Unfortunately, the existing high thermal conductivity copper alloys are wrought alloys and cannot be prepared by die casting [7−10], and the only die castable brass has a low thermal conductivity.

The key to designing the high thermal conductivity die-cast copper alloys lies in the selection of alloying elements. The addition of ordinary alloying elements to pure copper is prone to inclusions, poor strengthening effect and low thermal conductivity. Recently, rare earth (RE) elements have shown great advantages in alloying.

Corresponding author: De-jiang LI, Tel: +86-13918235110, E-mail: lidejiang@sjtu.edu.cn;
Xiao-qin ZENG, Tel: +86-18602108870, E-mail: xqzeng@sjtu.edu.cn
DOI: 10.1016/S1003-6326(23)66292-2

Adding a small amount of RE elements can purify the melt [11,12]. DANG et al [12] reported that adding 0.07 wt.% RE to pure copper effectively reduced the oxygen content from 0.1% to 0.006%. Adding a small amount of RE elements can effectively refine the microstructure. ZHOU et al [13] found that adding 0.15 wt.% La to Cu−0.25Te alloy reduced the grain size, which resulted in a simultaneous increase in strength and electrical conductivity. When RE is added as the main alloying element, it can significantly strengthen the alloy due to the formation of intermetallic compounds with high melting point and modulus. The advantages of purification, refinement and strengthening of some low solid solubility RE elements are very competitive when designing high thermal conductivity alloys.

The effects of alloying elements on the strengthening and thermal conductivity depend on their forms in the microstructure. Compared with solute atoms, intermetallic compounds can provide more significant strengthening effect and less reduction in thermal conductivity [14−16]. Therefore, the alloy element selected for forming intermetallic compound needs to have a minimum solid solubility in the matrix. At this point, the RE element lanthanum (La) is considered as one of the most promising candidates. La can easily react with Cu to form intermetallic compound Cu_6La (a simple monoclinic lattice: a=5.143 nm, b=10.204 nm and c=8.144 nm) [17] to strengthen pure copper due to their larger electronegativity difference (La, 1.10; Zr, 1.33; Cr, 1.66; Cu, 1.90) with Cu. Besides, the addition of La holds the high thermal conductivity of copper to most extent, due to the smallest limit solid solubility in the α-Cu matrix (La, 0 wt.% [18]; Cr, 0.70 wt.% [19]; Zr, 0.11 wt.% [19]). The grain boundary can be effectively strengthened by Cu_6La particles. However, the strength of α-Cu matrix needs to be improved, and solid solution strengthening (SSS) can be a good choice to solve this problem. CHEN and CHEN [20], and DINSDALE et al [21] found that Zn had the least effect on the thermal conductivity of copper alloys while strengthening the α-Cu matrix, which benefited from their similar properties (the same valence, 2.9% atomic mass difference, 14.7% atomic volume difference, and 0.25 electronegativity difference).

In this research, a series of Cu−La and Cu−2La−xZn alloys were prepared by gravity casting. Efforts were made to quantitatively study the effects of the Cu_6La intermetallic compounds and Zn solute atoms on the microstructure, hardness and thermal conductivity of binary Cu−La and ternary Cu−2La−xZn alloy systems, respectively. The thermal conductivity of Cu_6La was calculated, and the effect of Zn solute atoms on the thermal conductivity of the α-Cu matrix was quantified according to the results calculated by the Maxwell−Eucken model [22] based on the microstructure.

2 Experimental

Binary Cu−La and ternary Cu−2La−xZn alloys were prepared using pure copper (99.98 wt.%), pure lanthanum (99.98 wt.%) and Cu−30Zn master alloy in an induction furnace protected by high purity argon gas. Pure lanthanum (99.98 wt.%) and Cu−30Zn master alloy were added to the molten copper at 1200 °C. The molten alloys were poured into a mold preheated to 300 °C to obtain cylindrical ingots at 1150 °C. The chemical compositions of the ingots were determined by inductively coupled plasma-atomic emission spectroscopy (ICP-AES) and are listed in Table 1. The actual compositions were consistent with the expected compositions.

Table 1 Chemical compositions of experimental alloys in present work

Alloy	Content of La		Content of Zn		Content of Cu	
	wt.%	at.%	wt.%	at.%	wt.%	at.%
Cu−2.0La	2.12	0.98			Bal.	Bal.
Cu−2.5La	2.53	1.17			Bal.	Bal.
Cu−3.0La	2.98	1.38			Bal.	Bal.
Cu−3.5La	3.46	1.61			Bal.	Bal.
Cu−4.0La	4.11	1.92			Bal.	Bal.
Cu−4.5La	4.56	2.14			Bal.	Bal.
Cu−2La−0.1Zn	2.06	0.95	0.12	0.12	Bal.	Bal.
Cu−2La−0.25Zn	2.09	0.97	0.27	0.27	Bal.	Bal.
Cu−2La−0.5Zn	2.13	0.99	0.53	0.52	Bal.	Bal.
Cu−2La−1.0Zn	2.05	0.95	1.12	1.10	Bal.	Bal.
Cu−2La−2.0Zn	2.14	0.99	2.03	2.00	Bal.	Bal.
Cu−2La−3.0Zn	2.15	1.00	3.12	3.07	Bal.	Bal.

The Rigaku X-ray diffraction (XRD) with Cu $K_{\alpha 1}$ radiation was used to identify the intermetallic compounds and calculate the lattice constant of the α-Cu matrix with a scanning speed of 1 (°)/min, a voltage of 40 kV and a current of 30 mA. Metallographic samples were mechanically polished and etched with 4% HNO_3 for 8 s. Then, the samples were observed by a Zeiss Axio Observer A1 optical microscope (OM). Compositions of the α-Cu matrix and intermetallic compounds were further characterized by scanning electron microscopy (SEM) with energy dispersive spectroscopy (EDS) in back-scattered electron (BSE) mode, operated at an accelerating voltage of 15 kV. The volume fraction of intermetallic compounds was evaluated based on 10 OM images for each alloy using Image-Pro Plus software. The hardness of Cu−La alloys was characterized by a Vickers hardness tester (XHVT−10Z) with a loading force of 1.0 kg and a loading time of 15 s. The α-Cu matrix hardness of Cu−2La−xZn alloys was measured by an Agilent G200 XP Nanoindenter equipped with a Berkovich tip at room temperature, in displacement-controlled mode at a nominally constant strain rate of 0.05 s^{-1}, with a loading force of 10 g and a loading time of 5 s. The hardness value of each alloy was an average of 10 individual measurements.

Disc samples (12.70 mm in diameter and 2.50 mm in thickness) were machined from the alloys for thermal diffusivity measurements, using the laser flash method (Netzsch LFA 447) at 25 °C. The surface of the specimens was painted by a carbon coating before measurement to improve the absorption of the light pulse. The room temperature density of each alloy was obtained from an electronic balance (Sartorius Quintix124−1CN) with a densimeter (YDK03P), using the Archimedes method. The specific heat capacity of the alloys was measured by differential scanning calorimeter (DSC 2500). Thermal conductivity λ (W/(m·K)) was calculated as follows [23]:

$$\lambda=\alpha\rho c_p \quad (1)$$

where α is the thermal diffusivity (mm^2/s), c_p is the specific heat capacity (J/(g·K)) and ρ is the density (g/cm^3). The electrical conductivity of each alloy was measured by a Digital Eddy Current Metal Conductivity Instrument (Sigma 2008), and the average value of 5 individual measurements for each alloy was used to calculate the thermal conductivity according to the modified Weidmann−Franz law [24]:

$$\lambda=AL_0T\sigma+B \quad (2)$$

where A is a parameter, B is a constant associated with alloys, L_0 is the Lorentz constant, T is the thermodynamic temperature, and σ is the electrical conductivity. As for Cu alloys, A=0.967 [25], B= 7.53 W/(m·K) [25], and $L_0=2.33\times10^{-8}$ W·Ω/K^2 [26].

3 Results

3.1 Phase diagram and solidification path calculated by Pandat software

Figure 1(a) shows the phase diagram of the binary Cu−La alloy system. There are only two phases of α-Cu and Cu_6La, and only two kinds of structures including α-Cu and eutectic Cu_6La + Cu will be generated when the La content is low. Notably, the solid solubility of La in α-Cu is almost zero. As shown in Fig. 1(b), in the Cu−2La−xZn alloy system, the addition of Zn does not change the phase composition; nevertheless, only two phases of α-Cu and Cu_6La are generated, which just decrease the liquidus and solidus. However, the phase diagram can only provide equilibrium information, which deviates from the actual nonequilibrium solidification. To obtain better prediction results, the solidification paths of Cu−La and Cu−2La−xZn alloys were calculated by Pandat software, based on the nonequilibrium equation of Scheil's model. As shown in Fig. 1(c), the addition of La reduces the liquidus of Cu−La alloys and stabilizes the solidus at 853.5 °C due to the formation of eutectic Cu_6La intermetallic compounds. With increasing La content, the eutectic fraction increases approximately linearly. As shown in Fig. 1(d), in Cu−2La−xZn alloys, the addition of Zn reduces the solidus but hardly changes the phase fraction, which indicates that the fractions of α-Cu and eutectic Cu_6La do not change much.

3.2 Phase identification

Figure 2 shows the XRD patterns of the Cu−La and Cu−2La−xZn alloys. In the Cu−2La alloy, there are two phases of α-Cu and Cu_6La. With increasing La content, the phase composition does not change, but the diffraction peaks of Cu_6La are

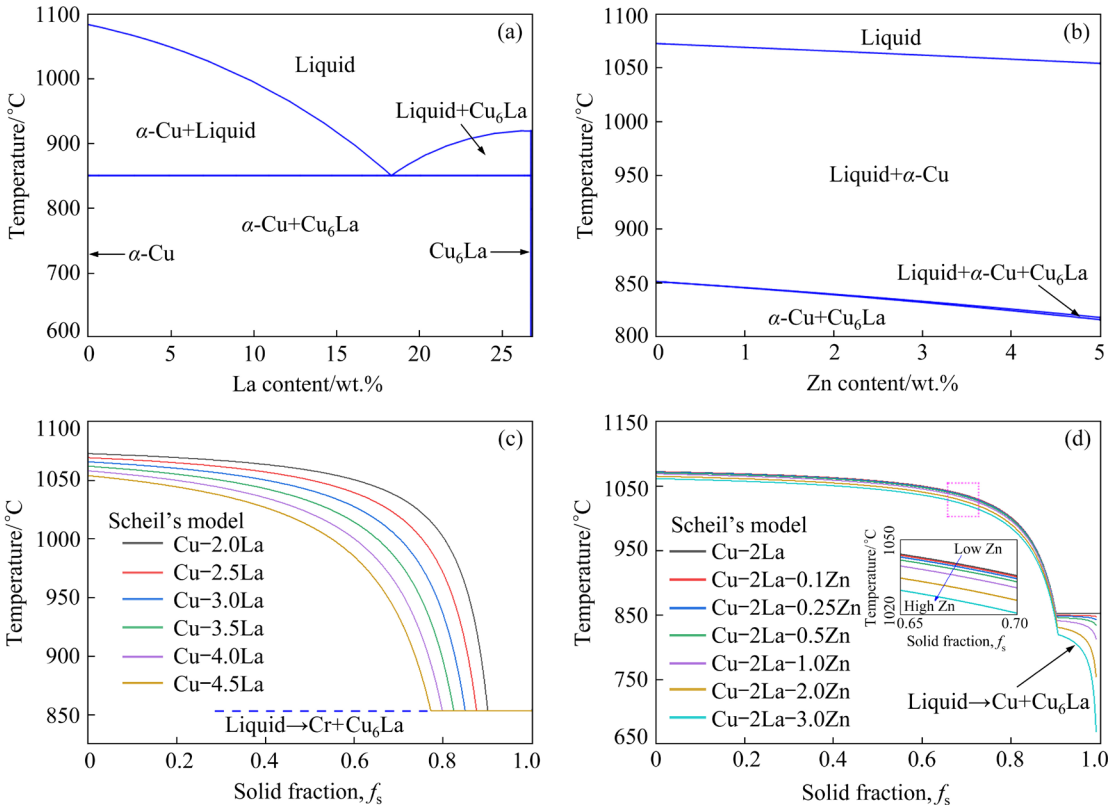

Fig. 1 Phase diagrams of binary Cu−La (a) and ternary Cu−2La−*x*Zn (b) alloy systems calculated by Pandat software, and solidification paths of Cu−La (c) and Cu−2La−*x*Zn (d) alloys calculated by Pandat software based on Scheil's model

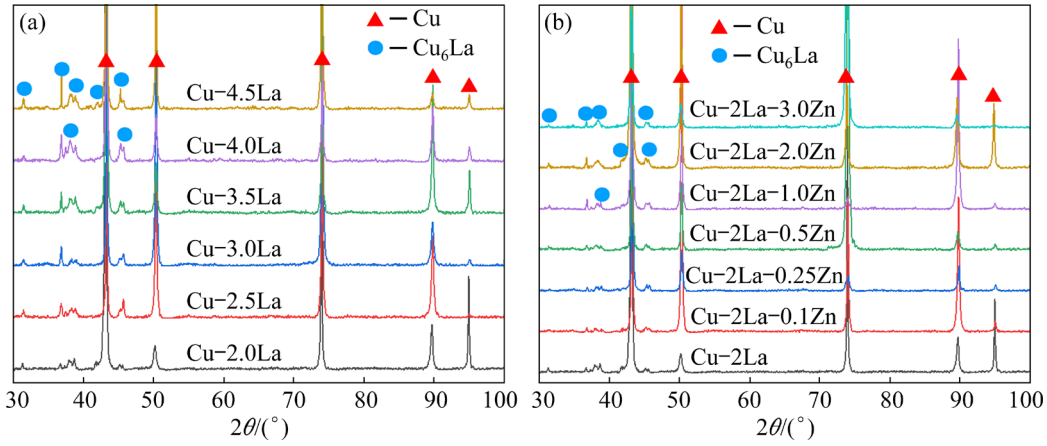

Fig. 2 XRD patterns of binary Cu−La (a) and ternary Cu−2La−*x*Zn (b) alloys

enhanced, which indicates that the Cu_6La volume fraction increases with increasing La content. In Cu−2La− *x*Zn alloys, as shown in Fig. 2(b), the addition of Zn does not change the phase composition. However, with increasing Zn content, the diffraction angles of *α*-Cu tend to shift to the left. According to Bragg's equation $2d\sin\theta=n\lambda'$ (*d* is the interplanar spacing, *θ* is the angle between the incident wave and the crystal plane, *n* is the integral multiple of wavelength, and *λ*′ is the incident wavelength), a smaller diffraction angle corresponds to a larger interplanar spacing and a larger lattice constant, which is due to the dissolution of Zn in the *α*-Cu matrix.

3.3 Microstructure and hardness

3.3.1 Microstructure evolution

Figure 3 presents the representative optical

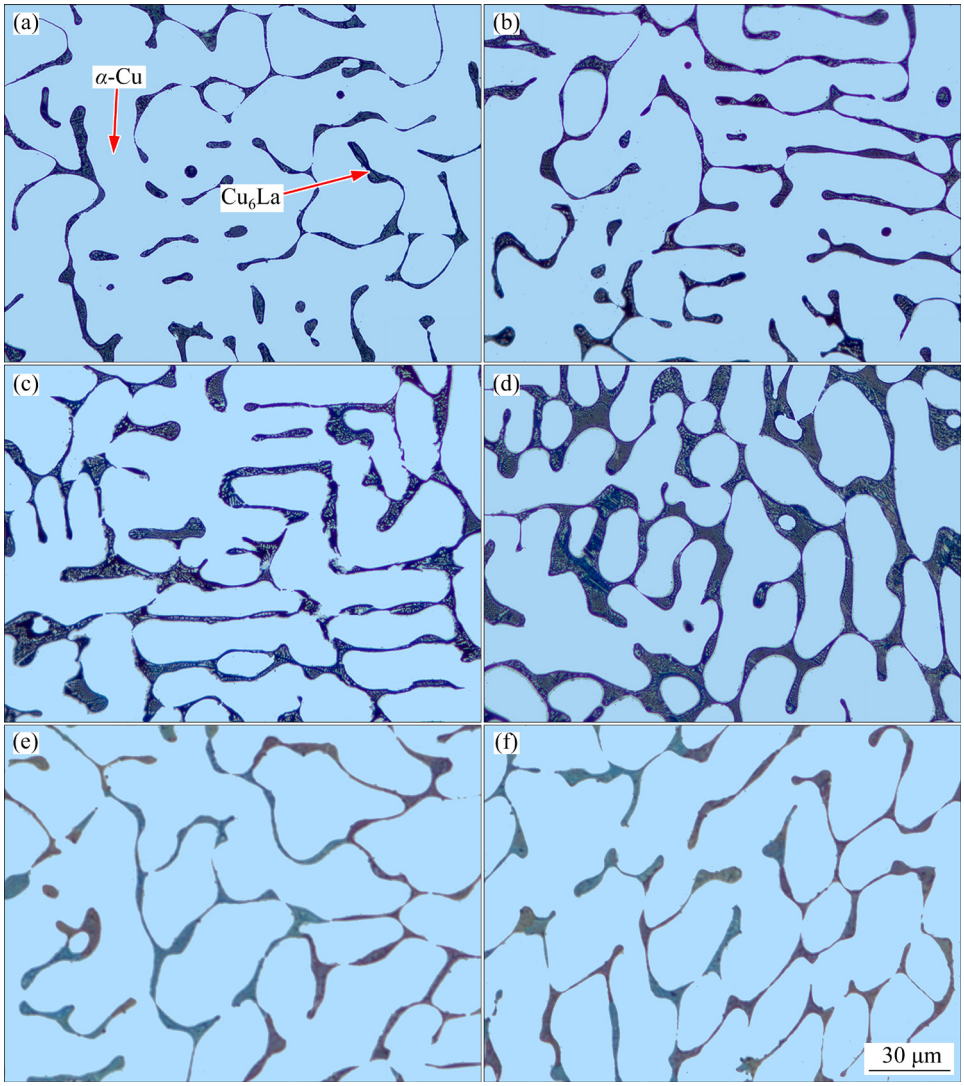

Fig. 3 Representative microstructures of Cu−2.0La (a), Cu−3.0La (b), Cu−4.0La (c), Cu−4.5La (d), Cu−2La−0.25Zn (e), and Cu−2La−3.0Zn (f) alloys

micrographs of the Cu−La and Cu−2La−*x*Zn alloys. Figure 3(a) shows that the microstructure of Cu−2La alloy is composed of an *α*-Cu matrix and eutectic Cu_6La intermetallic compounds. The phase composition remains unchanged when the La content increases to 4.5 wt.%, while the volume fraction of Cu_6La intermetallic compounds increases significantly. With increasing La content, the networked Cu_6La phase becomes wider. The volume fraction of Cu_6La presented in Table 2 was evaluated based on 10 OM images for each alloy using Image-Pro Plus software. The Cu_6La volume fraction increases from 7.55% to 18.63% with increasing La content from 2.0 wt.% to 4.5 wt.% in binary Cu−La alloys. Figures 3(a, e, f) imply that with increasing Zn content from 0 wt.% to 3.0 wt.% in Cu−2La-based alloys, there is little difference in the microstructure, which proves that the added Zn is only dissolved in the Cu matrix without forming intermetallic compounds. In addition, the Cu_6La volume fraction changes little with increasing Zn content, as presented in Table 3.

Table 2 Cu_6La content and hardness ($HV_{1.0}$) of microstructure in Cu−La alloys

Alloy	Cu_6La content/vol.%	Hardness ($HV_{1.0}$)
Cu−2.0La	7.55±1.13	74.43±1.11
Cu−2.5La	9.34±1.63	76.35±1.82
Cu−3.0La	11.51±1.52	81.25±1.50
Cu−3.5La	13.57±1.44	86.26±1.91
Cu−4.0La	16.65±1.23	92.83±1.53
Cu−4.5La	18.63±1.32	94.59±2.33

Table 3 Cu_6La content, Zn content in α−Cu matrix and hardness (H) of α−Cu matrix in Cu−2La−xZn alloys

Alloy	Cu_6La content/ vol.%	Zn content/ at.%	Hardness/ GPa
Cu−2La	7.55±1.13	0	1.495±0.025
Cu−2La−0.1Zn	7.22±0.81	0.12±0.03	1.513±0.022
Cu−2La−0.25Zn	7.36±0.89	0.26±0.02	1.521±0.031
Cu−2La−0.5Zn	7.34±1.10	0.53±0.04	1.530±0.028
Cu−2La−1.0Zn	7.63±0.90	1.03±0.12	1.548±0.041
Cu−2La−2.0Zn	7.23±0.52	2.12±0.11	1.573±0.032
Cu−2La−3.0Zn	7.12±0.83	3.05±0.05	1.597±0.037

As shown in Fig. 4, the matrix compositions of Cu−2La−xZn alloys were characterized and the Zn contents are presented in Table 3. The Zn contents in the matrix are close to the actual composition listed in Table 1. Based on the above observations and discussion, it can be confirmed that Zn atoms are entirely dissolved into the α-Cu matrix to form α-Cu solid solution for the present Cu−2La−xZn alloys. The EDS results indicate that the eutectic structure shown in Fig. 4(b) is composed of Cu_6La and Cu, in which Cu_6La accounts for the majority.

3.3.2 Hardness

To quantify the strengthening effects of La and Zn elements, the hardness of each alloy was characterized. As presented in Table 2, the hardness value of each Cu−La alloy was the average of 10 individual measurements. With increasing La content from 2.0 wt.% to 4.5 wt.%, the hardness value increases from $HV_{1.0}$ 74.43 to $HV_{1.0}$ 94.59 and presents a general linear growth trend. This results from the second phase strengthening of Cu_6La. For Cu−2La−xZn alloys, the effect of Zn on the hardness is not obvious, which may be masked if the Vickers hardness tester is used to characterize due to the hard Cu_6La phase. Therefore, the solid solution strengthening effect of Zn on the α-Cu matrix was characterized by an Agilent G200 XP Nanoindenter. The α-Cu matrix hardness values of Cu−2La−xZn alloys are presented in Table 3. With increasing Zn content from 0 to 3.0 wt.%, the hardness of the α-Cu matrix slowly increases from 1.495 to 1.597 GPa.

3.4 Data for calculating thermal conductivity

3.4.1 Density

Figure 5 shows the density values of Cu−La and Cu−2La−xZn alloys at 25 °C. As shown in Fig. 5(a), with increasing La content from 2.0 wt.% to 4.5 wt.%, the density slowly decreases from 8.8443 to 8.7763 g/cm^3. In general, the density of an alloy can be considered as the weighted average

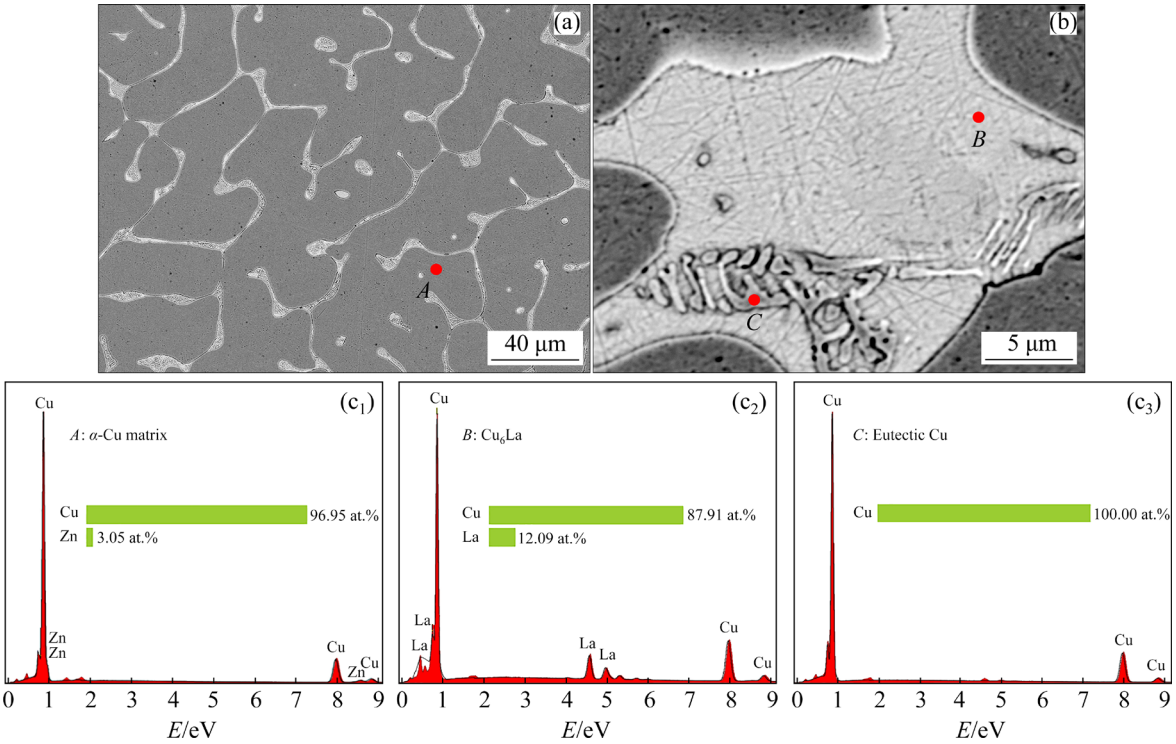

Fig. 4 SEM image of Cu−2La−3.0Zn alloy (a), eutectic structure in Cu−4.5La alloy (b), and EDS data of Positions A, B, and C (c_1−c_3)

of various phases. The density of Cu_6La is 8.07 g/cm^3, which is smaller than that of Cu (8.90 g/cm^3). Therefore, with increasing La content, the increasing volume fraction of Cu_6La results in a decreasing density of Cu−La alloys. Since the volume fraction of Cu_6La is almost unchanged, as shown in Table 3, the heavier Zn (65.38 g/mol, larger than that of Cu, 63.55 g/mol) atoms dissolved into the α-Cu matrix increase the density of Cu−2La−xZn alloys. However, the increase is very small, as shown in Fig. 5(b).

3.4.2 Specific heat capacity

As shown in Figs. 6(a, b), the specific heat capacity of each alloy was measured by differential scanning calorimeter, and the value of each alloy at 25 °C was calculated based on the results of linear

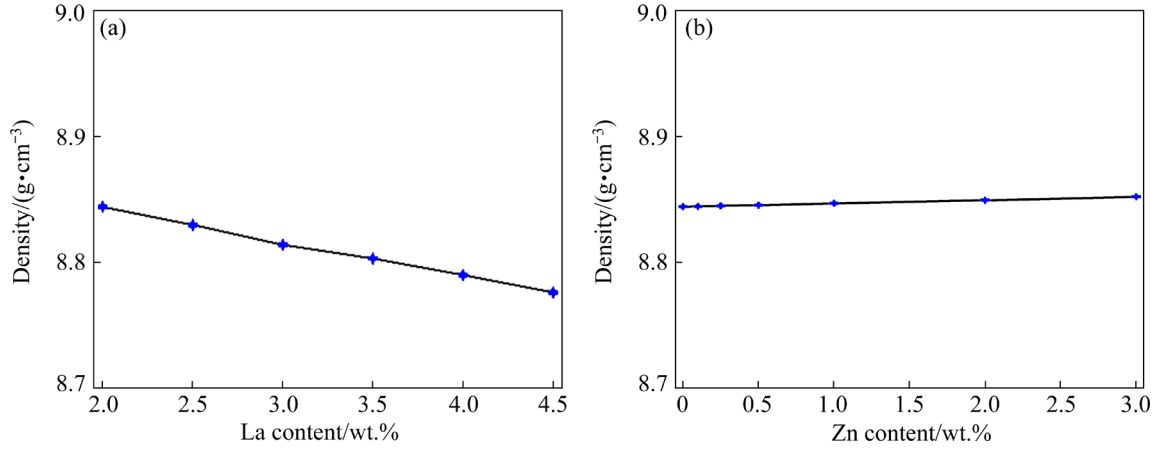

Fig. 5 Density values of Cu−La (a) and Cu−2La−xZn (b) alloys at 25 °C

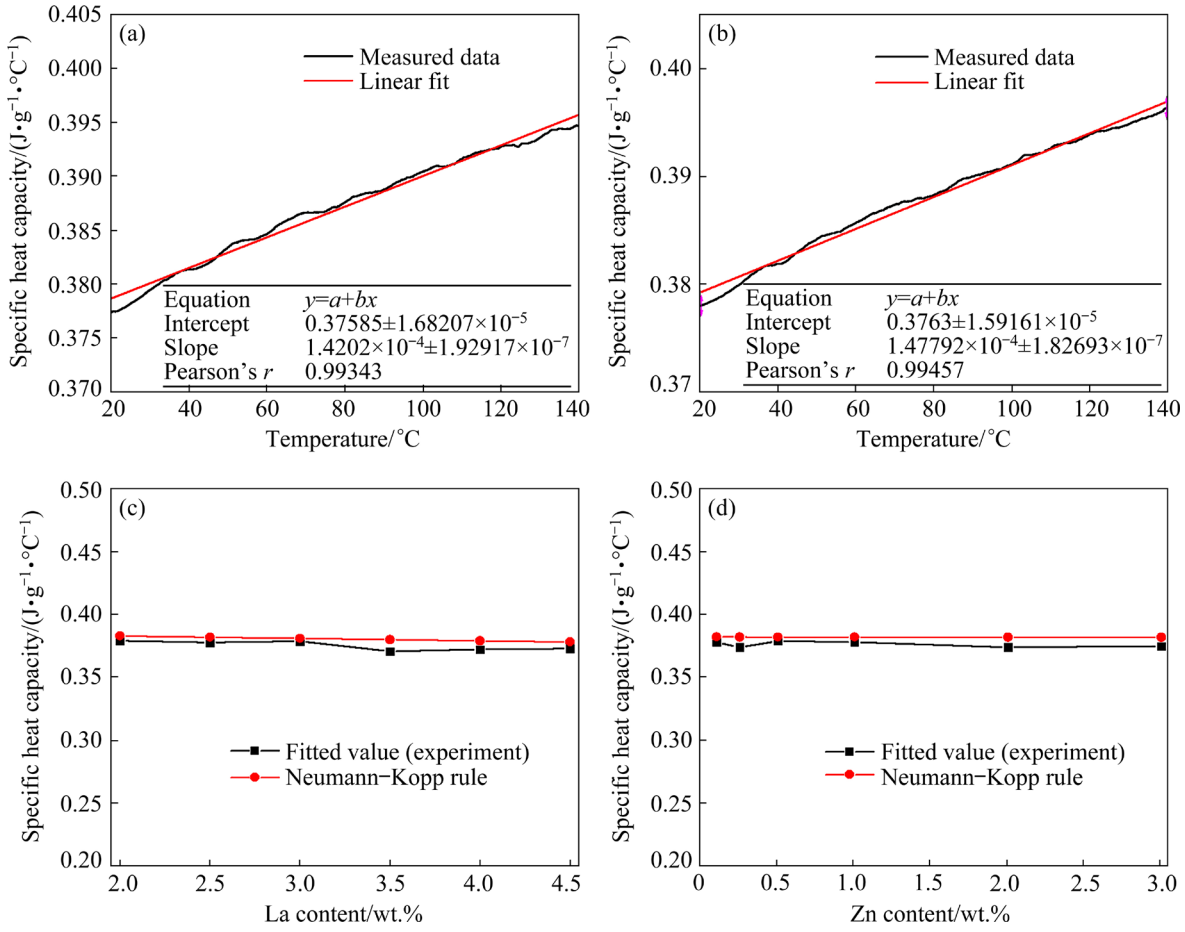

Fig. 6 Specific heat capacity vs temperature of Cu−2La (a) and Cu−2La−0.5Zn (b) alloys, and specific heat capacity of Cu−La (c) and Cu−2La−xZn (d) alloys at 25 °C

fitting from 20 to 140 °C. As shown in Figs. 6(c, d), the specific heat capacity changes little with increasing La or Zn content in the present work. The specific heat capacity (c_p) of Cu, La and Zn at 25 °C can be calculated by Eqs. (3)−(5) [27−29]:

$$c_p(\mathrm{Cu})=0.36+0.92\times10^{-4}T \quad (3)$$

$$c_p(\mathrm{La})=0.19+0.17\times10^{-4}T \quad (4)$$

$$c_p(\mathrm{Zn})=0.33+1.80\times10^{-4}T \quad (5)$$

The specific heat capacities of Cu−La and Cu−2La−xZn alloys were calculated using the Neumann−Kopp rule [30]:

$$c_p(T)=\sum c_{p,i}(T)x_i \quad (6)$$

where x is the mass ratio. Figures 6(c, d) show that the theoretical value hardly changes with increasing La (2.0−4.5 wt.%) and Zn (0−3.0 wt.%) contents in Cu−La and Cu−2La−xZn alloys, respectively. The experimental results are close to the calculation results.

3.4.3 Electrical conductivity and thermal diffusivity

In metal alloy materials, the conductive behavior is caused by the directional movement of free electrons. Generally, higher electrical conductivity is associated with more free electrons and less scattering. The thermal conductivity behavior also mainly depends on free electrons, and its change rule is consistent with the conductive behavior, so the electrical conductivity and thermal conductivity have a certain linear relationship. Thermal diffusivity represents the temperature diffusivity of an object, that is, the ability of an object to reach a steady state. The greater the thermal diffusivity is, the shorter the time for heat to diffuse from the local high temperature area to the low temperature area is. Thermal conductivity refers to the heat transfer per unit time and unit area, so it is proportional to the thermal diffusivity. As shown in Fig. 7, the electrical conductivity and thermal diffusivity decrease approximately linearly with increasing La content and Zn content in Cu−La and Cu−2La−xZn alloys, respectively. As shown in Fig. 7(a), the electrical conductivity decreases from 44.50 to 30.40 MS/m with increasing La content from 2.0 wt.% to 4.5 wt.% in Cu−La alloys, which approximately decreases by 5.64 MS/m for per 1.0 wt.% La. For the Cu−2La−xZn alloys shown in Fig. 7(b), the electrical conductivity deceases by 5.63 MS/m for per 1.0 wt.% Zn. The thermal diffusivity deceases by 9.00 and 9.91 mm^2/s per 1.0 wt.% La and Zn, respectively.

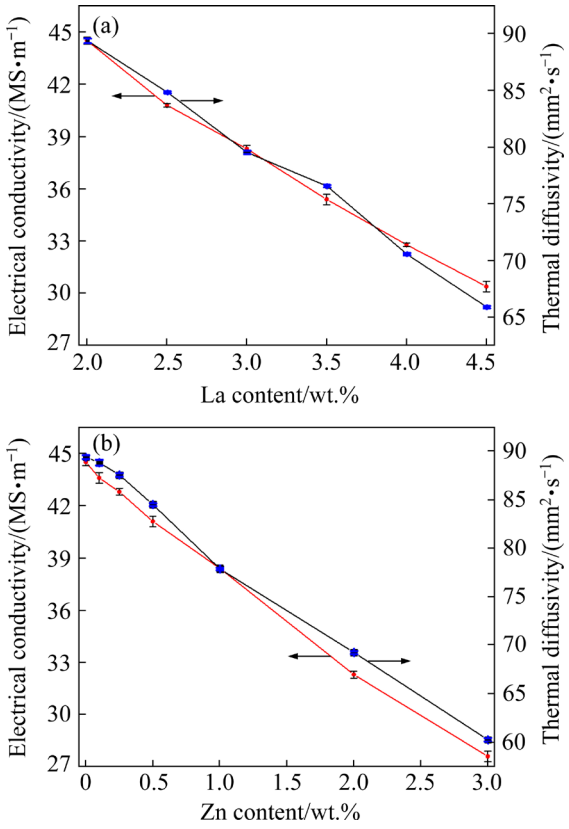

Fig. 7 Electrical conductivity and thermal diffusivity of Cu−La (a) and Cu−2La−xZn (b) at 25 °C

4 Discussion

4.1 Increase of α-Cu lattice constant of Cu−2La-based alloys by Zn solute atoms

As shown in Fig. 8(a), the diffraction angles of α-Cu present a decreasing trend with increasing Zn content in Cu−2La-based alloys. According to Bragg's equation, a decrease in 2θ means an increase in interplanar spacing. A substitutional solid solution will be formed when Zn atoms are dissolved in the α-Cu matrix. Since the atomic radius of Zn (134 pm) is larger than that of Cu (128 pm), the Zn solute atom increases the lattice constant of α-Cu. Eventually, the increase in lattice constant enlarges the interplanar spacing and then decreases the diffraction angles of α-Cu. The Nelson−Riley extrapolation function [31] is known as an accurate method to calculate the lattice constant of a crystal. Figures 8(b, c) show the method to calculate the lattice constant of α-Cu in Cu−2La and Cu−2La−1.0Zn alloys based on the diffraction angles obtained by XRD analysis. As shown in Fig. 8(d), the lattice constant of α-Cu increases from 361.63 to 362.39 pm (from 3.6163

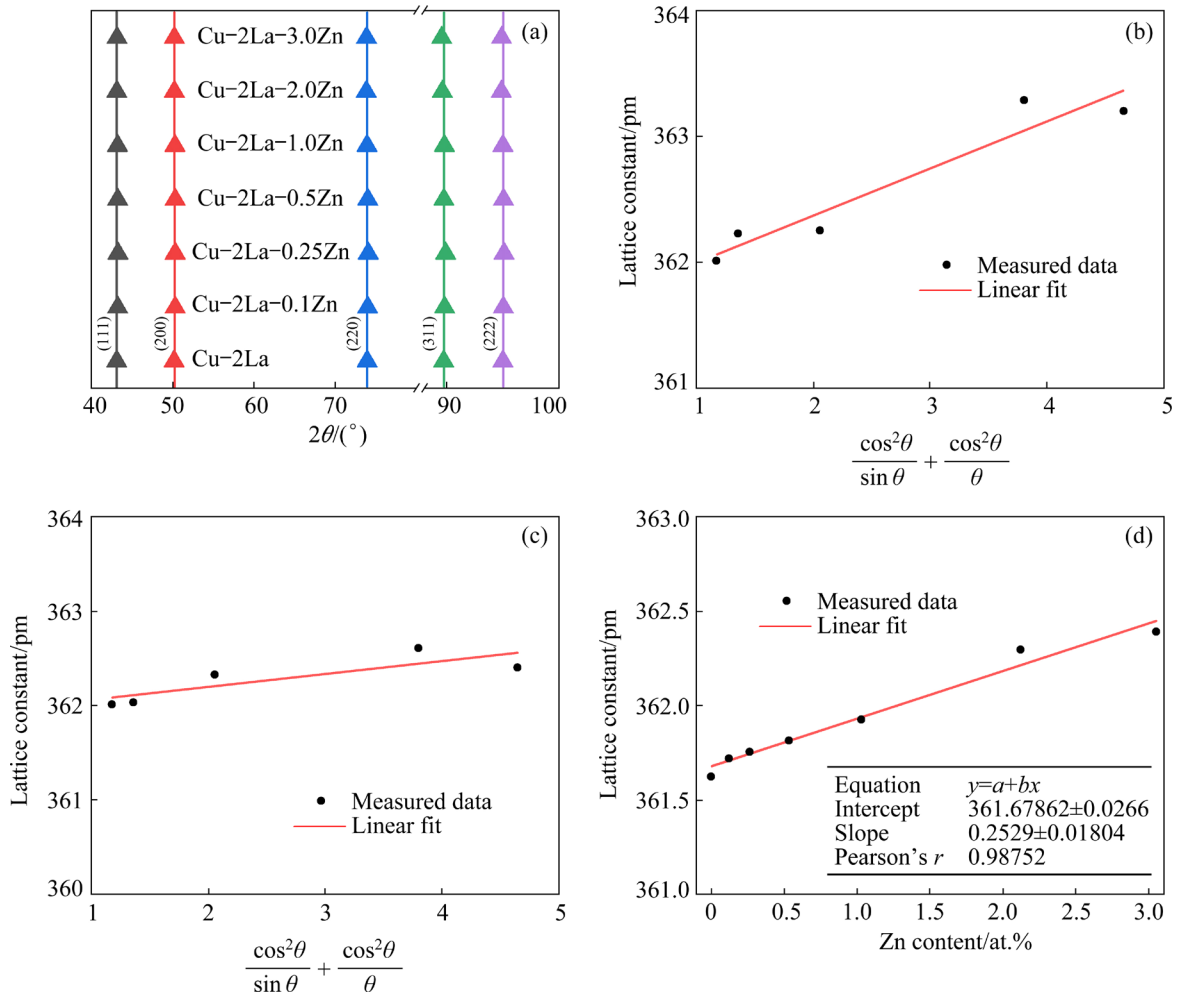

Fig. 8 Diffraction angles of α-Cu in Cu−2La−xZn alloys (a), lattice constants of α-Cu in Cu−2La (b) and Cu−2La−1.0Zn (c) alloys, and effect of Zn content on lattice constant of α-Cu in Cu−2La−xZn alloys (d)

to 3.6239 Å) as the actual solid solute Zn content increases from 0 to 3.05 at.%. The lattice constant of α-Cu increases linearly with increasing Zn content, approximately 0.25 pm per 1.0 at.% Zn solute atoms.

4.2 Effects of Cu_6La intermetallic compounds and Zn solute atoms on hardness of Cu−La−Zn alloys

4.2.1 Second phase strengthening

In the present work, the hardness of Cu−La alloys can be approximately calculated by using the weighted average of the two phases [32]:

$$H=f_1H_1+f_2H_2 \quad (7)$$

where H is the hardness of the alloy, f_1 and H_1 are the volume fraction and hardness of the matrix, respectively, and f_2 and H_2 are the volume fraction and hardness of the second phase, respectively. Since $f_1+f_2=1$, Eq. (7) can be rewritten as

$$H=f_2(H_2-H_1)+H_1 \quad (8)$$

In general, in the same alloy system prepared by the same process, the hardness value of the same phase is almost unchanged in the absence of solute atoms. Therefore, in Cu−La alloys, the hardness values of α-Cu and Cu_6La can be considered as constants. As shown in Fig. 9(a), the hardness of Cu−La alloys increases linearly with increasing Cu_6La volume fraction, which is consistent with the law given by Eq. (8). In addition, according to the fitting results, the hardness value of Cu_6La is approximately $HV_{1.0}$ 255.

4.2.2 Solid solution strengthening

As presented in Table 3, the hardness of the α-Cu matrix increases with increasing Zn solute atom content in Cu−2La−xZn alloys. Considering that the La content is constant and the solid solubility of La in α-Cu is zero in Cu−2La−xZn alloys, the solid solution strengthening effect should

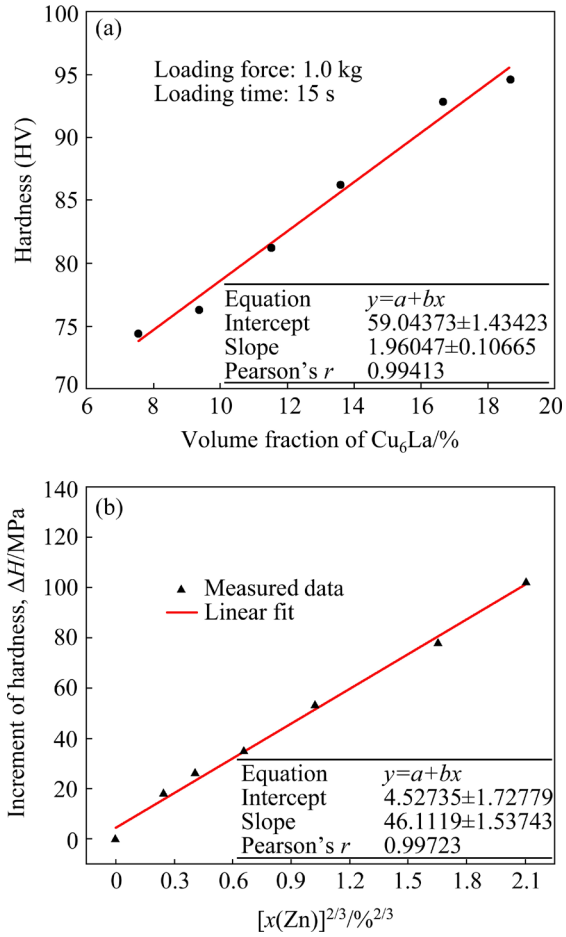

Fig. 9 Variation of hardness of Cu−La alloys with Cu_6La volume fraction (a) and hardness increment of α-Cu in Cu−2La−xZn alloys (b)

all be attributed to the Zn solute atoms. Since the larger Zn atoms replace the smaller Cu atoms to form substitutional solid solutions, distortions are generated in the crystalline network. These distortions hinder the dislocation movement [33] and increase the stress level correspondingly. According to the work of LABUSCH [34] and VOHRINGER [35], the contribution of solid solution strengthening (σ_{sss}) to the yield strength of Cu-based alloys can be calculated by using the following equation:

$$\Delta\sigma_{sss}=M\left(\frac{G}{550}\right)\varepsilon_L^{4/3}c_1^{2/3} \quad (9)$$

where M(=3.1) is the Taylor factor, G(=45 GPa) [36] is the shear modulus, c_1 is the solute fraction (at.%), and ε_L is

$$\varepsilon_L=\sqrt{(15\varepsilon_b)^2+\left(\frac{\varepsilon_G}{1+|\varepsilon_G|/2}\right)^2} \quad (10)$$

where the atomic size misfit (ε_b) and modulus misfit (ε_G) are given by $\varepsilon_b=(1/a)(da/dc)$ and $\varepsilon_G=(1/G)(dG/dc)$, respectively, and a and c are lattice constants. The contribution from the modulus effect was found to be negligible when the Zn solute atom content in the Cu matrix was low [37]. Therefore, in Cu−2La−xZn alloys, based on the lattice constant effect shown in Fig. 8(d), ε_L was calculated to be 1.037, and Eq. (9) can be calculated as [37,38]

$$\Delta\sigma_{sss}=kc_1^{2/3} \quad (11)$$

where k (=12.36 MPa/at.%$^{2/3}$) is the corresponding scaling factor. According to Tabor's relationship in Refs. [39−41], the increment in matrix hardness produced by solid solution strengthening can be expressed as follows:

$$\Delta H_{sss}=3\Delta\sigma_{sss}=3kc_1^{2/3} \quad (12)$$

In the present work, ΔH_{sss} was calculated according to the hardness value of each Cu−2La−xZn alloy presented in Table 3. As shown in Fig. 9(b), the increment in the hardness of the α-Cu matrix produced by solid solution strengthening and the Zn solute atom content satisfy the relationship of $\Delta H_{sss}=46.11c_1^{2/3}$. The corresponding scaling factor k is 15.37 MPa/at.%$^{2/3}$, which is close to the theoretical value of 12.36 MPa/at.%$^{2/3}$.

4.3 Effects of La and Zn contents on thermal conductivity of Cu−La−Zn alloys

As shown in Figs. 10(a, b), the thermal conductivity results calculated by the two methods are consistent. Since the data calculated by Eq. (1) reflects the thermal conductivity of the material better, the thermal conductivity calculated by Eq. (1) is used for discussion. As shown in Figs. 10(a, b), the thermal conductivity decreases by 33.88 W/(m·K) per 1.0 wt.% La in the Cu−La alloys, and that decreases by 33.72 W/(m·K) for per 1.0 wt.% Zn in Cu−2La−xZn alloys. The thermal conductivity of the Cu−La−Zn alloys can be described as follows:

$$\lambda_{(Cu-La-Zn)}=-33.88w(La)-33.72w(Zn)+367.78 \quad (13)$$

where La and Zn contents vary in the ranges of 2.0−4.5 wt.% and 0−3.0 wt.%, respectively.

4.3.1 Effects of Cu_6La intermetallic compounds and Zn solute atoms on thermal conductivity of Cu−La−Zn alloys

As shown in Figs. 10(a, b), although each increase of 1.0 wt.% La or Zn reduces the thermal conductivity of coper alloys by about 34 W/(m·K),

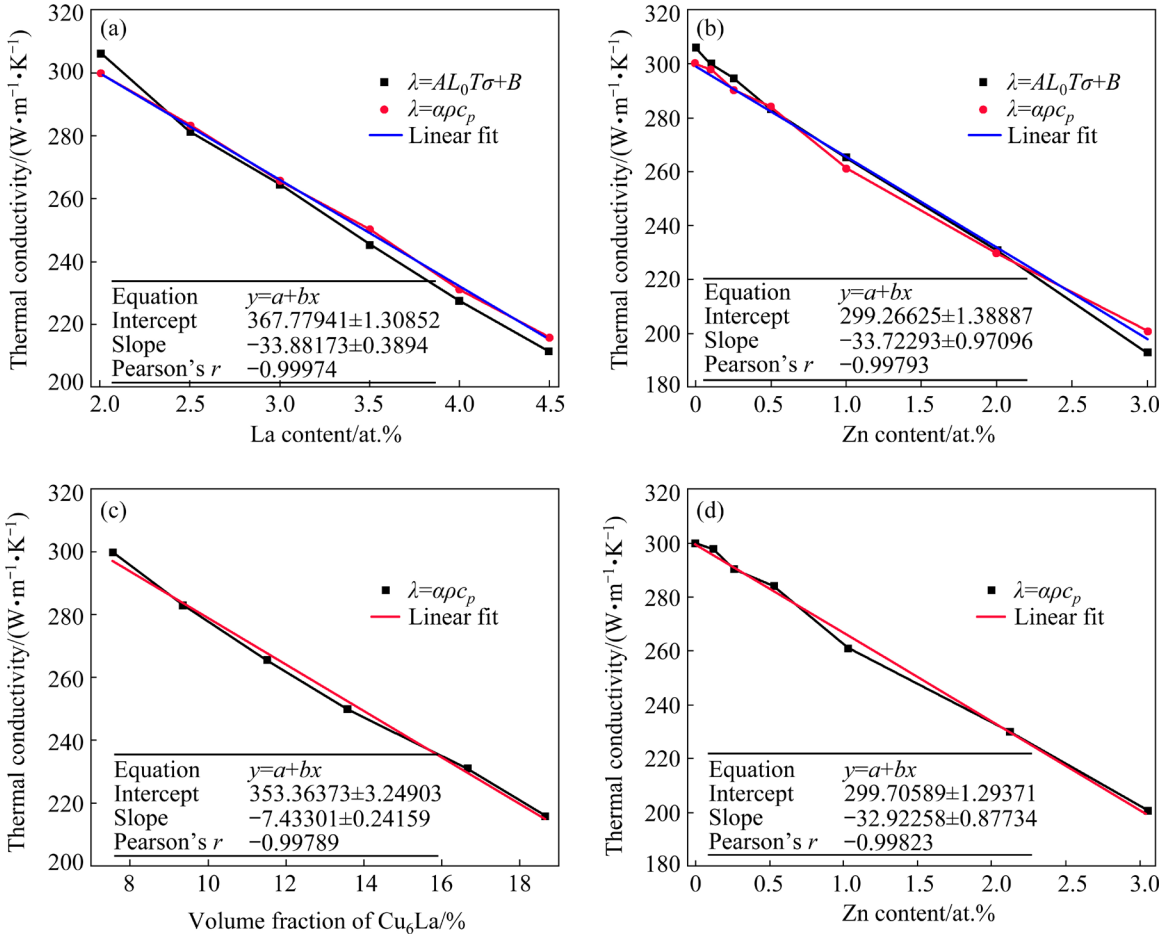

Fig. 10 Thermal conductivity of Cu−La (a) and Cu−2La−*x*Zn (b) alloys, variation of thermal conductivity of Cu−La alloys with Cu_6La volume fraction (c), and thermal conductivity of Cu−2La−*x*Zn alloys with mole fraction of Zn solute atoms (d) at 25 °C

their presence in the microstructure is completely different. Therefore, it cannot be considered that these elements have the same effect on the thermal conductivity of copper alloys. As shown in Fig. 10(c), the thermal conductivity of Cu−La alloys decreases approximately linearly with increasing Cu_6La volume fraction. The results show that the thermal conductivity decreases by approximately 7.43 W/(m·K) for increasing per 1.0% Cu_6La when the Cu_6La is distributed in a network in Cu−La alloys. As shown in Fig. 10(d), the thermal conductivity of Cu−2La−*x*Zn alloys also decreases linearly with increasing Zn solute atom content, which decreases by 32.92 W/(m·K) for every 1.0 at.% increase of Zn solute atoms.

4.3.2 Thermal conductivity of Cu_6La intermetallic compound

In the present work, the intermetallic compound Cu_6La is present in the form of a network surrounding the *α*-Cu grains, and the thermal conductivity can be estimated using the Maxwell−Eucken model [22]:

$$\lambda = \lambda_2 \frac{\lambda_1 + 2\lambda_2 - 2V_1(\lambda_2 - \lambda_1)}{\lambda_1 + 2\lambda_2 + V_1(\lambda_2 - \lambda_1)} \tag{14}$$

where λ_1 and λ_2 are the thermal conductivities of the *α*-Cu matrix and the Cu_6La intermetallic compound, respectively, and V_1 is the volume fraction of the *α*-Cu matrix. Since the solid solubility of La in the Cu matrix is zero, λ_1 is approximated as the thermal conductivity of pure copper (398 W/(m·K)). Therefore, in Eq. (14), there is only one unknown parameter λ_2 for binary Cu−La alloys in this work. According to the thermal conductivities of Cu−2.0La, Cu−2.5La, Cu−3.0La, Cu−3.5La, Cu−4.0La and Cu−4.5La, the thermal conductivities of Cu_6La in these alloys were calculated to be 34.43, 34.77, 35.40, 35.61, 36.56 and 35.44 W/(m·K), respectively. Because these six values are very close, the thermal conductivity of Cu_6La can be

considered to be the average of 35.37 W/(m·K).

4.3.3 Effect of Zn solute atoms on thermal conductivity of α-Cu matrix

Although Fig. 10(d) shows the effect of Zn solute atom content on the thermal conductivity of Cu−2La−xZn alloys, Zn solute atoms essentially first affect the thermal conductivity of the α-Cu matrix and then affect that of the alloy. Therefore, the thermal conductivities of the α-Cu matrix in Cu−2La, Cu−2La−0.1Zn, Cu−2La−0.25Zn, Cu−2La−0.5Zn, Cu−2La−1.0Zn, Cu−2La−2.0Zn and Cu−2La−3.0Zn were calculated to be 395, 386, 376, 365, 332, 280, and 237 W/(m·K), respectively. As shown in Fig. 11, the thermal conductivity of the α-Cu matrix in Cu−2La−xZn alloys decreases approximately linearly, which decreases by 51.38 W/(m·K) for every 1.0 at.% increase of Zn solute atoms.

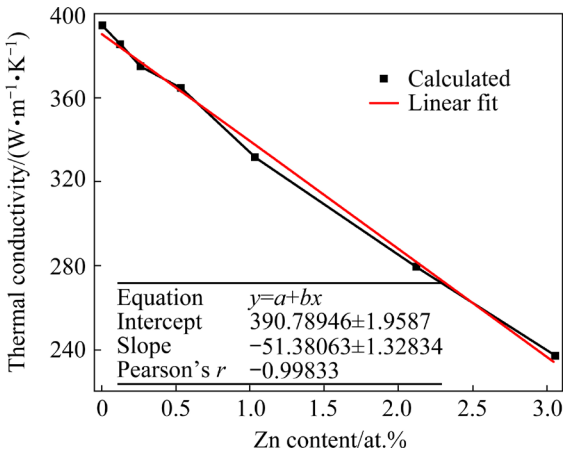

Fig. 11 Variation of thermal conductivity of α-Cu matrix with content of Zn solute atoms in Cu−2La−xZn alloys

5 Conclusions

(1) A new high thermal conductivity copper alloy system suitable for die casting was developed, which met the requirements of electronic component structural parts for high thermal conductivity and certain strength, and filled in the blank of high thermal conductivity die-casting copper alloys.

(2) With increasing Zn content from 0 to 3.0 wt.% in Cu−2La-based alloys, the lattice constant of α-Cu increased from 3.6163 to 3.6239 Å; the hardness of the α-Cu matrix increased from 1.495 to 1.597 GPa and was quantitatively expressed as ΔH=46.11$c_1^{2/3}$.

(3) The thermal conductivity of Cu−La−Zn alloys was quantitatively expressed as $\lambda_{(Cu-La-Zn)}$= −33.88w(La)−33.72w(Zn)+367.78, where La and Zn contents varied in ranges of 2.0−4.5 wt.% and 0−3.0 wt.%, respectively.

(4) The thermal conductivity of Cu−La alloys decreased by 7.43 W/(m·K) with increasing per 1.0 vol.% Cu_6La. The thermal conductivities of Cu−2La−xZn alloys and the α-Cu matrix decreased by 32.92 W/(m·K) and 51.38 W/(m·K), respectively, for every 1.0 at.% increase of Zn solute atoms.

Acknowledgments

This work was supported by the cooperation project between Shanghai Jiao Tong University and Huawei Technologies Co., Ltd., China, and the Major Science and Technology Projects of Yunnan Science and Technology Department, China (No. 202102AB080009). Xiao-qin ZENG would also like to acknowledge the support of the Xiao-qin ZENG Expert Workstation in Yunnan Province, China (No. 202005AF150059).

References

[1] LI Shu-bo, YANG Xin-yu, HOU Jiang-tao, DU Wen-bo. A review on thermal conductivity of magnesium and its alloys [J]. Journal of Magnesium and Alloys, 2020, 8: 78−90.

[2] LUO Gan, ZHOU Xiong, LI Cheng-bo, DU Jun, HUANG Zheng-hua. Design and preparation of Al−Fe−Ce ternary aluminum alloys with high thermal conductivity [J]. Transactions of Nonferrous Metals Society of China, 2022, 32: 1781−1794.

[3] SU Chuang-ye, LI De-jiang, LUO A A, YING Tao, ZENG Xiao-qin. Effect of solute atoms and second phases on the thermal conductivity of Mg−RE alloys: A quantitative study [J]. Journal of Alloys and Compounds, 2018, 747: 431−437.

[4] WANG Meng, YANG Qian-ru, JIANG Yan-bin, LI Zhou, XIAO Zhu, GONG Shen, WANG Yong-ru, GUO Chuang-li, WEI Hai-gen. Effects of Fe content on microstructure and properties of Cu−Fe alloy [J]. Transactions of Nonferrous Metals Society of China, 2021, 31: 3039−3049.

[5] WANG Meng-han, YANG Yong-chao, TU Shun-li, WEI Kang. A modified constitutive model and hot compression instability behavior of Cu−Ag alloy [J]. Transactions of Nonferrous Metals Society of China, 2019, 29: 764−774.

[6] HU Bo, QUAN Bei-bei, LI De-jiang, WANG Xue-yang, LI Zi-xin, ZENG Xiao-qin. Solid solution strengthening mechanism in high pressure die casting Al−Ce−Mg alloys [J]. Materials Science and Engineering A, 2021, 812: 141109.

[7] CALDATTO DALAN F, de LIMA ANDREANI G F, TRAVESSA D N, FAIZOV I A, FAIZOVA S, CARDOSO K R. Effect of ECAP processing on distribution of second phase particles, hardness and electrical conductivity of Cu−0.81Cr−0.07Zr alloy [J]. Transactions of Nonferrous Metals Society of China, 2022, 32: 217−232.

[8] PAN Zhen-ya, CHEN Jiang-biao, LI Jin-fu. Microstructure and properties of rare earth-containing Cu−Cr−Zr alloy [J]. Transactions of Nonferrous Metals Society of China, 2015, 25: 1206−1214.

[9] ZHANG Zi-chen, WANG Ri-chu, PENG Chao-qun, FENG Yan, WANG Xiao-feng, WU Xiang, CAI Zhi-yong. Effect of elevated-temperature annealing on microstructure and properties of Cu−0.15Zr alloy [J]. Transactions of Nonferrous Metals Society of China, 2021, 31: 3772−3784.

[10] ZHANG Shao-jian, LI Ren-geng, KANG Hui-jun, CHEN Zong-ning, WANG Wei, ZOU Cun-lei, LI Ting-ju, WANG Tong-min. A high strength and high electrical conductivity Cu−Cr−Zr alloy fabricated by cryorolling and intermediate aging treatment [J]. Materials Science and Engineering A, 2017, 680: 108−114.

[11] LI Hai-hong, LIU Xiao, LI Yang, ZHANG Shi-hong, CHEN Yan, WANG Song-wei, LIU Jin-song, WU Jin-hu. Effects of rare earth Ce addition on microstructure and mechanical properties of impure copper containing Pb [J]. Transactions of Nonferrous Metals Society of China, 2020, 30: 1574−1581.

[12] DANG Ping, ZHAO Lian-shan, LU Hua-yi, TANG Ding-xiang. Effect of rare earth on the microstructure and properties of pure copper [J]. Rare Metals, 1993, 12: 277−280.

[13] ZHOU Shi-jie, ZHAO Bing-jun, ZHAO Zhen, JIN Xin. Application of lanthanum in high strength and high conductivity copper alloys [J]. Journal of Rare Earths, 2006, 24: 385−388.

[14] TRITT T M. Thermal conductivity: Theory, properties, and applications [M]. New York: Kluwer Academic/Plenum Publishers, 2004: 21−91.

[15] BERMAN R. Thermal conduction in solids [M]. Oxford: Clarendon Press, 1976.

[16] EIVANI A R, AHMED H, ZHOU J, DUSZCZYK J. Correlation between electrical resistivity, particle dissolution, precipitation of dispersoids, and recrystallization behavior of AA7020 aluminum alloy [J]. Metallurgical and Materials Transactions A, 2009, 40: 2435−2446.

[17] CHEN Yan, CHENG Ming, SONG Hong-wu, ZHANG Shi-hong, LIU Jin-song, ZHU Yan. Effects of lanthanum addition on microstructure and mechanical properties of as-cast pure copper [J]. Journal of Rare Earths, 2014, 32: 1056−1063.

[18] DU Zhen-min, XU Yun-hua, ZHANG Wei-jing. Thermodynamic assessment of the Cu−La system [J]. Journal of Alloys and Compounds, 1999, 289: 88−95.

[19] LIU Yu-ling, ZHOU Peng, LIU Shu-hong, DU Yong. Experimental investigation and thermodynamic description of the Cu−Cr−Zr system [J]. Calphad, 2017, 59: 1−11.

[20] CHEN Shu-chuan, CHEN Ling-bing. Physical properties of materials [M]. Shanghai: Shanghai Jiao Tong University Press, 1999: 40. (in Chinese)

[21] DINSDALE A, KHVAN A, SMIRNOVA E A, PONOMAREVA A V, ABRIKOSOV I A. Modelling the thermodynamic data for hcp Zn and Cu−Zn alloys: An ab initio and calphad approach [J]. Calphad, 2021, 72: 102253.

[22] MAXWELL J. A treatise on electricity and magnetism [M]. Cambridge: Oxford University Press, 1904.

[23] ZHANG Wan-peng, MA Ming-long, YUAN Jia-wei, SHI Guo-liang, LI Yong-jun, LI Xing-gang, ZHANG Kui. Microstructure and thermophysical properties of Mg−2Zn−*x*Cu alloys [J]. Transactions of Nonferrous Metals Society of China, 2020, 30: 1803−1815.

[24] POWELL R W. Correlation of metallic thermal and electrical conductivities for both solid and liquid phases [J]. International Journal of Heat and Mass Transfer, 1965, 8: 1033−1045.

[25] SMITH C, PALMER E. Thermal and electrical conductivities of copper alloys [J]. AIME Technical Publications and Contributions, 1935, 648: 1−19.

[26] ZHANG Fan, GUO Yi-ping, ZHOU Wei-ming. Properties of materials [M]. 2nd ed. Shanghai: Shanghai Jiao Tong University Press, 2015: 297. (in Chinese)

[27] BRANDES E A, BROOK G B. Smithells metals reference book [M]. 7th ed. Bath: Great Britain, 1992: 8−41.

[28] TOULOUKIAN Y S. Thermophysical properties of matter [M]. New York: IFI/Plenum Press, 1970.

[29] TOULOUKIAN Y S. Specific heat: Metallic elements and alloys [M]. New York: IFI/Plenum Press, 1970: 50−300.

[30] GONG Wei-ping, LIU Yan-zhi, LUO Zhi-hong. Heat capacity of samarium titanates and phase equilibria of Sm_2O_3−TiO_2 system [J]. Journal of Alloys and Compounds, 2021, 860: 158429.

[31] NELSON J B, RILEY D P. An experimental investigation of extrapolation methods in the derivation of accurate unit-cell dimensions of crystals [J]. Proceedings of the Physical Society, 1945, 57: 160−177.

[32] HU Geng-xiang, CAI Xun, RONG Yong-hua. Fundamentals of materials science [M]. 3rd ed. Shanghai: Shanghai Jiao Tong University Press, 2010: 188−191. (Chinese)

[33] DIETER G E. Mechanical metallurgy [M]. London: McGraw-Hill Book Company, 1988.

[34] LABUSCH R. A statistical theory of solid solution hardening [J]. Physica Status Solidi, 1970, 41: 659−669.

[35] VOHRINGER O. The influence of alloy type and concentration on the yield point of alpha-copper alloys [J]. Zeitschrift fuer Metallkunde, 1974, 65: 352−358.

[36] SARMA V S, SIVAPRASAD K, STURM D, HEILMAIER M. Microstructure and mechanical properties of ultra fine grained Cu−Zn and Cu−Al alloys produced by cryorolling and annealing [J]. Materials Science and Engineering A, 2008, 489: 253−258.

[37] FRIEDEL J. Dislocations [M]. Oxford: Pergamon, 1964.

[38] NABARRO F R N. Theory of crystal dislocation [M]. Oxford: Oxford University Press, 1967.

[39] TABOR D. The hardness of metals [M]. Oxford: Clarendon Press, 1951.

[40] LABUSCH R, GRANGE J A G, HAASEN P. Rate processes in plastic deformation of materials [M]. Cleveland: American Society for Metals, 1975.

[41] TODA-CARABALLO I. A general formulation for solid solution hardening effect in multicomponent alloys [J]. Scripta Materialia, 2017, 127: 113−117.

铸造 Cu−La−Zn 合金的强化及导热行为

胡 波[1]，韩嘉璇[1]，李德江[1,2]，于铭迪[1]，王静雅[1]，王雪杨[1]，李子昕[1]，黄 彧[3]，曾小勤[1,2]

1. 上海交通大学 材料科学与工程学院 轻合金精密成型国家工程研究中心，上海 200240；
2. 上海交通大学 金属基复合材料国家重点实验室，上海 200240；
3. 华为技术有限公司，深圳 518129

摘 要：开发一种适合于压铸的高导热 Cu−La−Zn 合金，该合金的导热系数高达 200~300 W/(m·K)，约为普通黄铜的两倍。分别定量研究铸态二元 Cu−La (2.0%~4.5% La，质量分数)和三元 Cu−2La−*x*Zn (0~3.0% Zn，质量分数)合金中 Cu_6La 金属间化合物和 Zn 固溶原子对强化和导热行为的影响。结果表明：每增加 1%(质量分数)的 La 或 Zn，合金导热系数下降约 34 W/(m·K)。Cu−2La−*x*Zn 合金中 *α*-Cu 基体的晶格常数随 Zn 固溶原子的增加由 3.6163 Å 增加到 3.6239 Å；在 Zn 原子的固溶强化作用下，*α*-Cu 基体的硬度由 1.495 GPa 呈抛物线增加至 1.597 GPa。根据基于显微组织的 Maxwell−Eucken 模型计算结果，确定 Cu_6La 的导热系数约为 35.37 W/(m·K)；而每增加 1% Zn(摩尔分数)的固溶原子，*α*-Cu 基体的导热系数下降 51.38 W/(m·K)。

关键词：Cu−La−Zn 合金；强化；导热系数；金属间化合物；固溶原子

(Edited by Wei-ping CHEN)